Following the Electrochemical Oxidation of Au(111) in Real-Time Using Surface Optical Reflectance and Total-Reflection X-Ray Absorption

Downloaded from: https://research.chalmers.se, 2026-05-10 07:46 UTC

Citation for the original published paper (version of record):

Grespi, A., Larsson, A., Abbondanza, G. et al (2026). Following the Electrochemical Oxidation of Au(111) in Real-Time Using Surface Optical
Reflectance and Total-Reflection X-Ray Absorption Spectroscopy. Journal of the Electrochemical Society, 173(7). http://dx.doi.org/10.1149/1945-7111/ae5bcf

N.B. When citing this work, cite the original published paper.

research.chalmers.se offers the possibility of retrieving research publications produced at Chalmers University of Technology. It covers all kind of research output: articles, dissertations, conference papers, reports etc. since 2004. research.chalmers.se is administrated and maintained by Chalmers Library

(article starts on next page)

Journal of The
Electrochemical Society

OPEN ACCESS

Following the Electrochemical Oxidation of Au(111) in Real-Time Using Surface Optical Reflectance and Total-Reflection X-Ray Absorption Spectroscopy

To cite this article: A. Grespi *et al* 2026 *J. Electrochem. Soc.* **173** 076502

View the article online for updates and enhancements.

You may also like

- Enhancing the Performance of Zero-Excess Lithium Metal Batteries: A Contribution to a Practical Guide
Tjark T. K. Ingber, Marian C. Stan, Martin Winter et al.
- Wettability Determination of Gas Diffusion Layers for Polymer Electrolyte Fuel Cells
Barbara Thiele, Juan Herranz, Thomas J. Schmidt et al.
- Preventing On-Farm Antibiotic Toxicity: A Green Polyaniline Potentiometric Sensor for On-Farm Monitoring of Valnemulin
Mennatallah H. Eltahawy, Hala E. Zaazaa, Shereen Mowaka et al.

The New PAT-Cell-Solid!

EL-CELL® electrochemical test equipment

Cycle Solid-State Batteries Under Controlled Pressure of up to 300 MPa (6 mm Diameter)!

- Adjust and measure a force of up to 9000 N on the cell stack!
  Force adjustment possible throughout the entire experiment
- Built-in force, and temperature sensors!
  With optional gas pressure sensor and gas in- and outlet
- PAT-Solid-Core for easy assembly and reproducible results!
  Press and cycle solid-state batteries with 6 or 10 mm electrode diameter
- Cableless and highly sealed battery test cell!
  For precise long-term measurements of solid-state cell chemistries

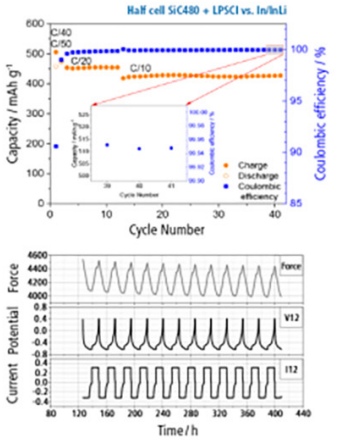

Learn more on our product website: Scan me!

Download the data sheet (PDF): Scan me!

Or contact us directly:
+49 40 79012-734
sales@el-cell.com
www.el-cell.com

This content was downloaded from IP address 94.234.68.83 on 24/04/2026 at 08:20

Journal of The Electrochemical Society, 2026 **173** 076502

Following the Electrochemical Oxidation of Au(111) in Real-Time Using Surface Optical Reflectance and Total-Reflection X-Ray Absorption Spectroscopy

A. Grespi,[1,2,z] A. Larsson,[3] G. Abbondanza,[4] J. Manidi,[5] J. Eidhagen,[6] E. Lira,[1,2] A. Ti,[1,2] M. Ramakrishnan,[7] J. Just,[7] J. Pan,[8] L. R. Merte,[9,2] and E. Lundgren[1,2]

[1]*Division of Synchrotron Radiation Research, Lund University, Box 118, 22100 Lund, Sweden*
[2]*NanoLund, Lund University, Box 118, 22100 Lund, Sweden*
[3]*Leiden Institute of Chemistry, Leiden University, Leiden, The Netherlands*
[4]*Department of Physics, Chalmers University of Technology, Chalmersplatsen 4, 41296 Gothenburg, Sweden*
[5]*Politecnico di Milano, Department of Chemistry, Materials and Chemical Engineering, G. Natta, 20133 Milano, Italy*
[6]*Alleima AB, SE-811 34 Sandviken, Sweden*
[7]*MAX IV Laboratory, Lund University, Lund, Sweden*
[8]*KTH Royal Institute of Technology, Division of Surface and Corrosion Science, Stockholm, Sweden*
[9]*Materials Science and Applied Mathematics, Malmö University, 20506 Malmö, Sweden*

Under electrochemical polarization, many electrocatalysts can undergo oxidation that alters their reactivity and can lead to restructuring and dissolution. In this context, the structure-property relationships of electrocatalysts, as well as their kinetics and dynamic behaviour, are still poorly understood. This knowledge gap mainly relies on the limitations of many traditional spectroscopic and structure determination methods, which cannot be easily coupled in situ with electrochemical methods. In this work, we performed cyclic voltammetry (CV) combined with 2D surface optical reflectance (2D-SOR) and total reflection X-ray absorption spectroscopy (RefleXAFS) in a single *operando* experiment, to directly follow the electro-oxidation and reduction of a Au(111) model electrode. Our results show that the surface in 0.05 M H_2SO_4 forms a self-limiting Au^{3+} oxide or hydroxide film around 1.5 V_{RHE} during the anodic scan in the CV (2 mV s^{-1}), with a thickness of ~5 Å estimated from the 2D-SOR measurements. The film is then rapidly reduced during the cathodic scan around 1.1 V_{RHE}.
© 2026 The Author(s). Published on behalf of The Electrochemical Society by IOP Publishing Limited. This is an open access article distributed under the terms of the Creative Commons Attribution 4.0 License (CC BY, https://creativecommons.org/licenses/by/4.0/), which permits unrestricted reuse of the work in any medium, provided the original work is properly cited. [DOI: 10.1149/1945-7111/ae5bcf]

Manuscript submitted February 4, 2026; revised manuscript received March 31, 2026. Published April 14, 2026.

Supplementary material for this article is available online

Many important electrochemical (EC) reactions occur at EC potentials where the surface of electrodes may be oxidized, such as the Oxygen Evolution Reaction (OER),[1,2] Oxygen Reduction Reaction (ORR),[3] and EC oxidation of Methanol,[4] CO,[5] and Glucose.[6] It has been shown that changes in red-ox chemistry at the surface alters the reactivity [1,5,7] or selectivity [4,8] of reactions and can be coupled to dissolution and hence catalyst degradation.[9,10] These complex processes originate at the electrode-electrolyte interface and their atomic and molecular scale understanding can provide useful insights to design more efficient and cost-effective electrocatalysts.[4,8,11,12] However, traditional electro-analytical tools, e.g. impedance spectroscopy and sweep voltammetry,[13,14] despite successful, do not directly provide such detailed and precise information.[15–17] Therefore, it is essential to use complementary experimental methods that allow to study the dynamic evolution of model electrodes surfaces under relevant conditions, ideally during the EC measurements, to unveil the details of the surface behaviour with a multimodal approach.[18–22]

2D surface optical reflectance (2D-SOR) is emerging as a versatile, powerful and cost-effective method to directly image model surfaces in harsh reactive environments with sub-nanometer surface sensitivity.[23–25] Deconvoluting the contributions to the overall reflectance changes is essential to advance and spread the use of this technique and a suitable approach is combining 2D-SOR with other time-resolved surface-sensitive methods to study model systems. To this end, advances in synchrotron radiation instrumentation and experimental methodologies have enhanced prevailing *operando* surface-sensitive techniques, unlocking new possibilities and perspectives for X-ray studies in heterogeneous catalysis,[21,26–29] thereby paving the way to explore the electrified solid-liquid interface with soft X-rays, e.g. ambient pressure XPS (AP-XPS),[18,28,30,31] or hard X-rays, e.g. high-energy surface X-ray diffraction (HESXRD),[19,32] and total-reflection X-ray absorption fine structure spectroscopy (RefleXAFS).[33–36] In the case of surfaces or substrate-supported thin films and nanoparticles, the signal can be enhanced by focusing the incoming X-ray beam on the sample surface, in the so-called grazing incidence (GI) geometry.[21,26,37,38] Provided a sufficiently flat and smooth surface, i.e. mirror-polished, if the grazing angle is set below the critical angle for total external reflection, the X-rays will exhibit the lowest penetration depth in the material.[33,39,40] However, at very shallow incident angles the footprint of e.g. a 100 μm wide X-ray beam on the sample can be several millimetres, hence, this configuration requires a precise alignment in all directions, using a stable and extremely focused beam.[41,42] Finally, the sample size and the sample environment need to be designed carefully to accommodate the X-ray beam footprint, while avoiding excessive attenuation of the X-ray beam through the electrolyte.[41,42] In these conditions, fluorescent detected X-ray absorption fine structure under grazing incidence (GI-XAFS) was shown to be a powerful spectroscopic method for *operando* experiments in heterogeneous catalysis and electrochemistry.[37,42–45] However, GI-XAFS has been only used for nanoparticles and thin films supported by a substrate of a different material, since it can be measured in fluorescence mode unhindered by any scattering from the substrate.[37,42–45] In the case of thick samples where the surface and the bulk contain the same species, e.g. single crystals or industrial alloys, the fluorescence signal from the surface cannot be easily distinguished from that of the bulk.[33] Provided a flat and smooth surface, RefleXAFS can be used to minimize the substrate contribution, by measuring the reflected beam intensity as a function of the incident beam energy.[33,46–49] Particularly, the possibility to use this method under electrochemical conditions to obtain surface information was demonstrated for sputtered metal films[34,50] and it was only recently shown to be suitable for thick model electrodes.[33,36]

[z]E-mail: andrea.grespi@sljus.lu.se

Au single crystals have been commonly used as model electrodes to investigate the fundamental steps in electrocatalytic reactions,[51] e. g. to study the oxidation of methanol,[52] CO,[53] and glucose.[54] All these reactions take place at high anodic potentials, where the gold surface can be oxidized. In a previous study on the electro-oxidation of Au(111) model electrode in acidic electrolyte, the same EC cell used in this experiment was employed for *operando* time-resolved HESXRD and 2D surface optical reflectance (2D-SOR).[23,32] Thanks to the high beam energy used in the HESXRD experiment (60–80 keV), the attenuation through the electrolyte is significantly lowered and the size of the Ewald sphere is increased, simplifying and accelerating the data acquisition process.[26,32] As a result, the HESXRD measurements revealed a steep decrease in the Au(111) crystal truncation rods (CTR) signal intensity accompanied by a steep decrease in the 2D-SOR intensity when the potential reaches ca. 1.5 V_{RHE} during cyclic voltammetry (CV) at 10 mV s^{-1} in 0.1 M $HClO_4$.[32] At this potential, an anodic current peak is observed in the CV and an ultra-thin gold oxide/hydroxide film has been claimed to form on the Au(111) surface, before significant OER current is observed (OER onset).[1,55–57] However, although HESXRD and 2D-SOR suggest that oxidation and reduction dynamics can be monitored with relatively high time-resolution, the surface structural information from HESXRD is limited: CTR intensities quickly drop and there is no direct evidence of any new structural feature associated to any hydroxide/oxide formation, as also observed on Pt.[17,58] This is believed to result from the amorphous nature of these hydroxide/oxide thin films forming on the surface.[32,34,59] Due to the ambiguity in literature about the nature of these hydroxides, oxides or hydrated-oxides phases, we will generally refer to them as (hydr-) oxides.

As an alternative to HESXRD, RefleXAFS can be used to detect directly the oxidation and reduction of a model gold electrode under constant anodic polarization[33] and recently we have shown that this can be done even dynamically during CV.[36] Although an energy-dependent X-ray reflectance model is needed to accurately quantify the amount of near-surface species using RefleXAFS, the cationic character of the surface was clearly revealed by an increase of the so-called absorption "white line" intensity at the Au L_3-edge.[60–62] In the present study, we combine for the first time in a single experiment time-resolved RefleXAFS and 2D-SOR to directly follow the electro-oxidation and reduction of Au(111) during CV in 0.05 M H_2SO_4 at 2 mV s^{-1}. The RefleXAFS data presented in this work belong to our recent multimodal study[36] and are here complemented by 2D-SOR to demonstrate their capabilities and to estimate the (hydr-)oxide film thickness. We show that the Au(111) surface quickly forms an ultra-thin Au^{3+} (hydr-)oxide during the anodic (upward) scan around 1.5 V_{RHE}, displaying a self-limiting behaviour. The thickness for a Au_2O_3 film formed above 1.5 V_{RHE} is estimated from the changes in 2D-SOR intensity to be around ∼5 Å and is discussed in comparison to the EC current and RefleXAFS measurements. Finally, besides surface oxidation and reduction phenomena, we discuss the additional surface changes revealed by 2D-SOR as a function of potential in the light of existing surface structure models.

Methods

A schematic of the poly-ether ether ketone (PEEK) EC flow-cell combined with RefleXAFS and 2D-SOR used at the Balder beamline of MAX IV (Lund, Sweden) is shown in Fig. 1. The EC cell and 2D-SOR are well described in previous studies,[23,33,63,64] with wall thickness of 200 μm. The EC cell and 2D-SOR setup are mounted on top of a goniometer with the hat-shaped sample surface sitting parallel to the polarization direction of the beam. The 2D-SOR images were acquired at a frame rate of 1 Hz and were normalized dividing all the raw images by the initial raw image acquired at the open circuit potential (OCP) when the surface appeared in a metallic state. For RefleXAFS measurements, each spectrum was recorded in 5 s and it was not necessary to merge several spectra to obtain sufficiently good signal-to-noise ratio. The calculation of the critical

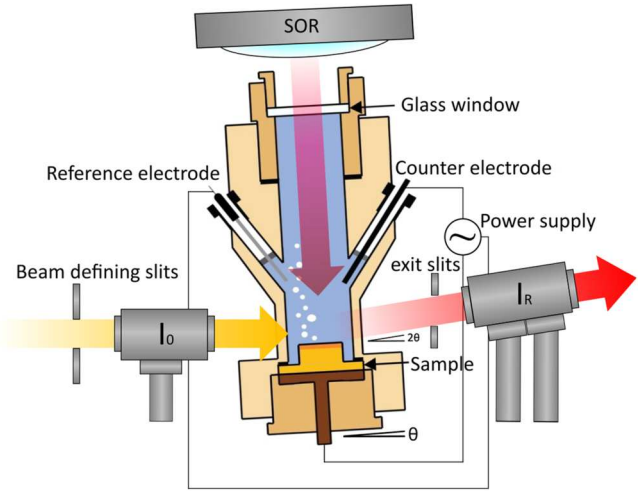

Figure 1. Schematic of the EC flow cell combined with 2D-SOR and RefleXAFS setup used at the Balder beamline of MAX IV (Lund, Sweden), adapted from Ref 36.

angle for a thick gold substrate at the interface with ultra-high vacuum (UHV), H_2O or H_2SO_4 using the Au L_3-edge beam energy (11919 eV) are reported in the supplementary information (SI) (Table S1), showing values above 0.3° (∼5.2 mrad). The incident angle used in this experiment was set to 0.2° (∼3.5 mrad). The incident beam (I_0) horizontal size was set to a full-width half maximum (FWHM) of 100 μm and the vertical size to a FWHM of 12 μm, which provides a beam footprint of approximately 3.5 mm, well below the sample surface diameter of 7.5 mm. The Ionization chamber to measure the totally reflected beam (I_R) was tilted by approximately 0.2° and then the angular acceptance was defined by horizontal and vertical slits placed between the EC cell and the ionization chamber. Both ionization chambers (to measure respectively I_0 and I_R) were filled with 0.1 bar of Ar and 1.9 bar of N_2.

For easy visualization and comparison with the reference X-ray absorption near-edge spectra (XANES) measured in transmission mode, the energy-dependent reflectance is normalized in the same way as a traditional XANES data treatment,[35,65,66] i.e. normalizing the $-\ln(I_R/I_0)$ as shown in Fig. S1. Due to the nature of the reflection process and the anomaly in the refractive index close to an absorption edge, the contribution of edge features to the RefleXAFS spectra can arise from both the contribution of the evanescent wave absorption process as well as transmission through island-like features under shallow incidence and reflection angle. For an incidence angle far below the critical angle the spectral shape of the absorption fine structure comes close to traditional transmission data.[49,50] Significant deviations of the RefleXAFS features measured in total reflection compared to traditional reference XANES are indeed not evident in our data. While disentangling the individual contributions for fully quantitative determinations is in focus of our future work, we here perform a rather qualitative comparison to normal reference transmission spectra and take advantage of 2D-SOR to quantify the (hydr-)oxide thickness. The reference XANES spectra were measured in transmission mode from a Au foil provided at the beamline, and from pellets of Au_2O_3 and $Au(OH)_3$ powders purchased from American Elements® (US). The powders were exposed to ambient air at room temperature during the pellet preparation and during measurements, while cellulose was used as a binder.

The single-crystalline Au(111) sample was provided by Surface Preparation Laboratory (SPL, Netherlands) and the top-most surface was mirror polished from SPL with an average roughness Ra <0.03 μm. After polishing and prior to the experiment, the sample was flame annealed with a butane torch and subsequently cooled in air. The EC cell and tubing system were cleaned with 30/70 v/v HNO_3(65%)/H_2SO_4(96%) solution followed by rinsing with

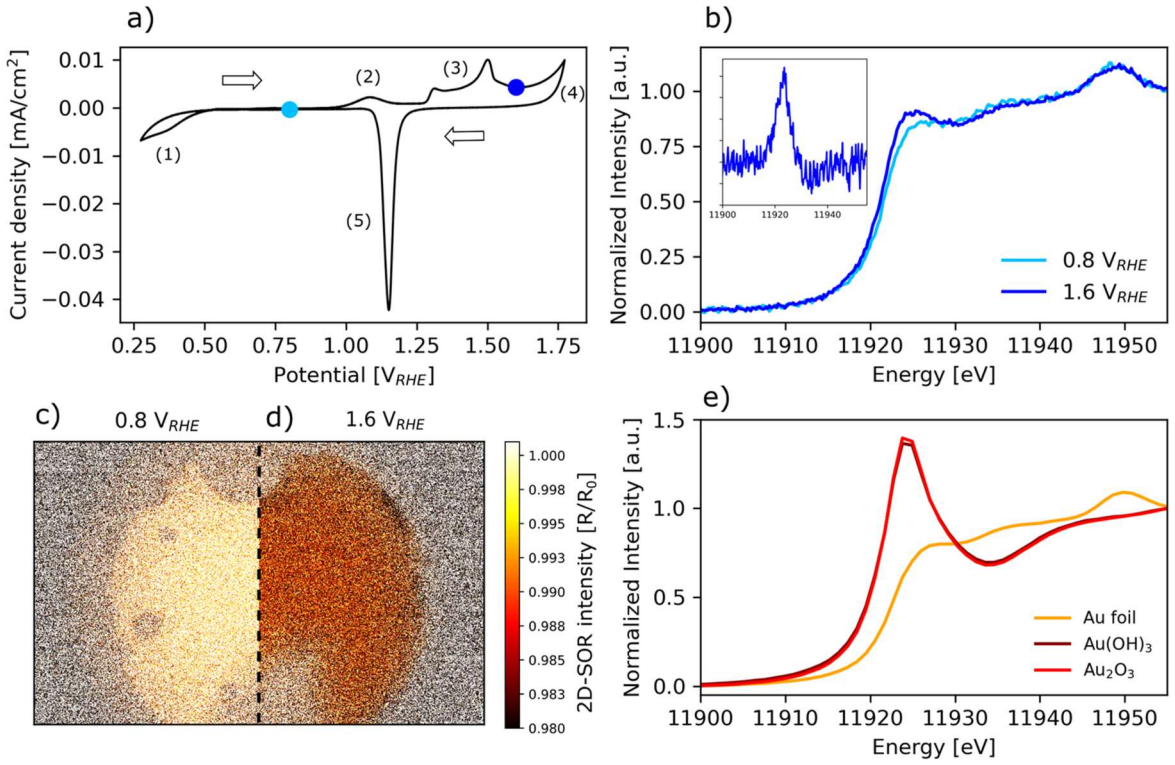

Figure 2. (a) The first CV at 2 mV s^{-1} in 0.05 M H_2SO_4 between 0.27 and 1.77 V_{RHE} during the time-resolved experiment. The arrows show the directions of the scan, the blue dots correspond to the potential where the RefleXAFS spectra shown in (b) and the 2D-SOR images shown in (c) and (d) were obtained. (b) Example of the normalized time-resolved RefleXAFS spectra measured at 0.8 V_{RHE} and 1.6 V_{RHE} during the upward CV scan. To highlight the white line intensity increase, the inset shows the difference between the two spectra. (c), (d) Normalized 2D-SOR images measured during the CV at the two potentials corresponding to the spectra shown in (b). The intensity is normalized to the reflectance at OCP. (e) Reference XANES spectra of Au foil and Au_2O_3 and $Au(OH)_3$ pellets.

ultrapure Milli-Q H_2O (mQ, 18.2 MΩ) boiling water. The glassware was cleaned with a 50/50 v/v HNO_3(65%)/H_2SO_4(96%) solution followed by rinsing cycles with mQ boiling water. The electrolyte was prepared with Suprapur® H_2SO_4(96%) and mQ and then purged with Ar bubbling for at least 1 hour before the experiment.

The EC measurements were performed using an Autolab PGSTAT101 potentiostat. A Pt rod was used as counter electrode, and an eDAQ ET072–1 leakless miniature Ag/AgCl was used as reference electrode (RE), which was first calibrated with respect to a standard Ag/AgCl RE. The time-resolved experiment was performed in static electrolyte and consisted of 2 CV cycles performed at 2 mV s^{-1} in the potential window 0.27–1.77 V_{RHE}, while measuring 2D-SOR and RefleXAFS. The CV shown in this work is not iR-compensated. We notice here that the sides of the single-crystal are exposed to the electrolyte and thus contribute to the overall voltametric response (at least 50% of the total surface area).

Results and Discussion

Figure 2a shows the first of the two CV cycles of Au(111) in 0.05 M H_2SO_4 in the range 0.27–1.77 V_{RHE} at 2 mV s^{-1} performed during the time-resolved measurements. The arrows in Fig. 2a indicate the directions of the anodic (upward) and cathodic (downward) scans of the CV. The two blue coloured dots correspond to the potentials in the anodic (upward) scan at which the time-resolved RefleXAFS spectra shown in Fig. 2b were measured. The inset of Fig. 2b shows the difference between the two spectra. Figures 2c and 2d show the 2D-SOR images obtained during the time-resolved measurements at the potentials corresponding to the RefleXAFS spectra shown in Fig. 2b. The reference XANES spectra of Au_2O_3, $Au(OH)_3$ and Au foil are shown in Fig. 2e, where $Au(OH)_3$ shows the same XANES features of Au_2O_3 and are used here as a reference for Au^{3+} species.

As can be observed in the CV of Fig. 2a, almost no current is measured between 0.5 V_{RHE} and 0.9 V_{RHE}, supposedly because this region lies where there should only be the current associated to the charging and restructuring of the EC double layer (EDL).[67,68] Below 0.5 V_{RHE}, an increasing cathodic current is observed (1) and is attributed to the oxygen reduction reaction (ORR) from the small amount of dissolved oxygen left in the electrolyte.[33] During ORR, O_2 can be converted to H_2O ($4e^-$ pathway) or to H_2O_2 ($2e^-$ pathway) depending on the selectivity of the catalysts, electrolyte pH and applied potential.[69] Differently from e.g. Pt, Au is more likely to undergo both pathways, reducing O_2 to both H_2O and H_2O_2.[70] In fact, the anodic peak observed in the upward scan around 1.1 V_{RHE} (2) could be associated to oxidation of the produced H_2O_2, as also observed in previous studies.[70] At higher potentials, the characteristic so-called oxidation peaks (3) of Au are revealed between 1.3 V_{RHE} and 1.6 V_{RHE}, where each gold facet is expected to oxidize at a discrete potential depending on the surface orientation.[55,71] Since the sides of the single crystal are also exposed to the electrolyte, additional oxidation peaks appear in this potential range close to the Au(111) oxidation peak, but our surface sensitive methods allow to identify the potentials where oxidation of the Au(111) surface take place. At higher potentials in Fig. 2a, the further increase of the current above 1.75 V_{RHE} (4) is attributed to the OER onset.[1] During the cathodic (downward) scan, a current peak (5) is observed around 1.1 V_{RHE}, commonly attributed to the reduction of the (hydr-)oxide.[9,72]

As can be seen in Fig. 2b, the main change observed in the RefleXAFS spectra is the small increase of the white line intensity around 11923 eV, which is indicative of a cationic character present at the surface.[33,60,73] To emphasize the increase of the white line intensity, the inset in Fig. 2b shows the difference RefleXAFS spectrum obtained by subtracting the spectrum at 0.8 V_{RHE} from the spectrum at 1.6 V_{RHE}, as also shown in Fig. S2. For comparison, also

the difference reference XANES for the Au_2O_3 pellet is plotted in Fig. S2, where the metallic reference XANES spectrum of the Au foil is subtracted from that of the Au_2O_3 pellet. Despite some uncertainties about the exact near-edge XAFS features of differently oxidized Au-species, Au^{3+} ions are expected to largely influence the white line intensity.[33,60,73] Indeed, a clear increase of the white line intensity is observed in the reference XANES of the Au_2O_3 and $Au(OH)_3$ pellets (Fig. 2e) and is highlighted in the difference reference XANES (Fig. S2), suggesting that the surface could be oxidized to a 3+ state, as proposed by previous density functional theory and surface-enhanced Raman spectroscopy studies.[1] These details are further disclosed in our recent work.[36] In conjunction with the increase of the white line intensity described above, a clear decrease in the 2D-SOR intensity is observed (Figs. 2c, 2d) during the anodic (upward) scan, which can be attributed to a change of the surface refractive index due to its oxidation.[32,71]

As a summary of the entire time-resolved RefleXAFS experiment, a complete dataset of the normalized RefleXAFS spectra during the two CV cycles in the potential range between 0.27 and 1.77 V_{RHE} is shown in Fig. S3. Figures 3b and 3c show the changes of the RefleXAFS white line and 2D-SOR intensities during the CV scan. The white line intensity is calculated as the area integrated under the first peak in the difference RefleXAFS spectra around 11923 eV, e.g. the peak shown in the inset of Fig. 2b. The integrated area is then normalized to the area integrated from the difference reference XANES shown in Fig. S2a, in this manner a 100% increase of the RefleXAFS white line intensity would be what is expected for a thick (hydr-)oxide, where the entire absorbing volume would only consist of Au^{3+} species, as a reference. The 2D-SOR intensity is calculated from the blue ROI shown in Fig. S4 and is normalized with respect to the ROI intensity at OCP. Finally, the plot of the 2D-SOR intensity is smoothened using a kernel smoothing function with a moving average of 50 datapoints. Additional ROIs have been chosen for comparison, all of them showing the same trend (Fig. S4). Sped up movies of the related time-resolved 2D-SOR and RefleXAFS measurements during the CV cycles are uploaded as supplementary material.

In Fig. 3b during the anodic (upward) scan, a steep increase of the white line intensity is observed around 1.5 V_{RHE}, in correspondence of the main oxidation peak in Fig. 3a, and is thus attributed to a quick oxidation of the Au(111) surface. These results are in good agreement with previous studies on Au(111) using EC scanning tunnelling microscopy,[74] 2D-SOR[23,32] and HESXRD.[23,32] Above 1.5 V_{RHE}, the (hydr-)oxide signal only slightly increases while approaching the OER onset (4), this suggests a self-limiting behaviour of the thin (hydr-)oxide film in this potential region.[13] As the potential scan is reversed downward (cathodic scan), the white line intensity is stable, until it quickly reduces when the reduction potential is approached (5). The drop of the RefleXAFS signal is sharp and coincides exactly with the reduction peak in the CV (5). Finally, at low potentials in Fig. 3b, the white line intensity does not show significant changes during ORR (1) as well as in the entire EDL region, suggesting that the RefleXAFS measurements were not sensitive to the small changes of the near-edge features expected for e.g. the adsorption and desorption of oxygenated species and the lifting of the surface reconstruction taking place in the EDL region.[32,67,75] On the contrary, in this low potential region the 2D-SOR measurements exhibit a small linear decrease of the intensity with increasing polarization, further discussed below.

In Fig. 3c, the overall trend of the 2D-SOR intensity during the oxidation-reduction of the surface is inversely correlated to that of the white line intensity, and it agrees well with the previous 2D-SOR

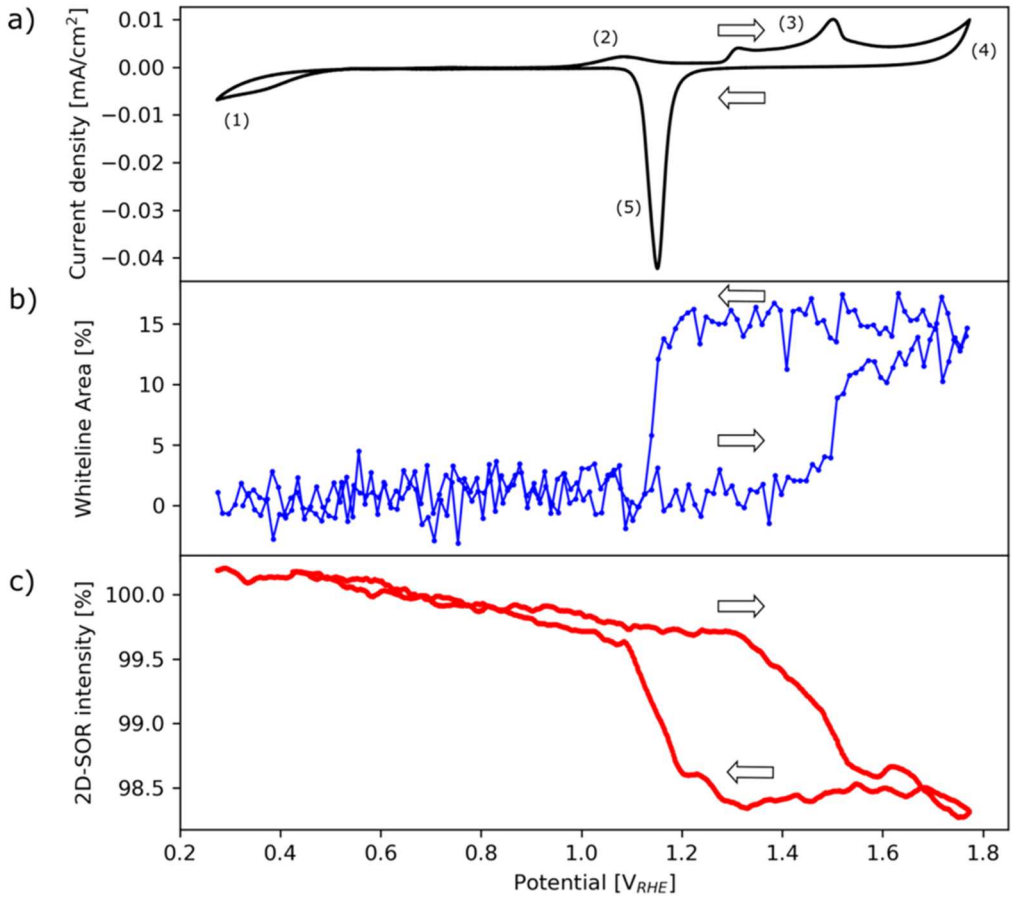

Figure 3. (a) CV of Au (111) in 0.05 M H_2SO_4 in the range 0.27–1.77 V_{RHE} at 2 mV s^{-1}. (b) RefleXAFS white line intensity normalized to the intensity of the reference XANES. (c) 2D-SOR intensity normalized to the reflectance at OCP.

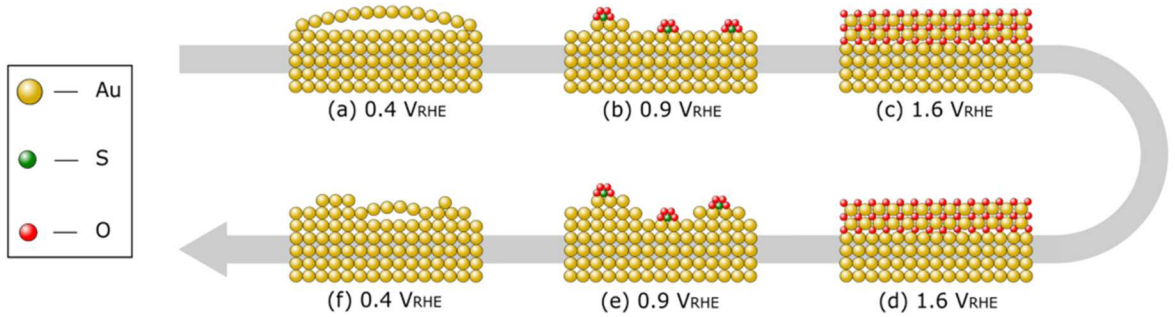

Figure 4. Ball models of the Au(111) surface during the CV in 0.05 M H_2SO_4, inspired by Kondo et al.[75]

studies during CV on Au(111) in H_2SO_4 and $HClO_4$.[32,64] However, a small linear decrease of the SOR intensity with increasing polarization is observed in the low potential region, and might be attributed to the adsorption/desorption of oxygenated species and the reconstruction of the surface in the ORR and EDL regions,[32,76] as shown in the proposed atomic model (Fig. 4) inspired by Kondo et al.[75] According to the previous XRR[75] and HESXRD[32] studies, the pristine surface exhibits the typical herringbone-like surface reconstruction below ca. 0.5–0.6 V_{RHE} in the anodic (upward) scan (Fig. 4a). In this potential region the 2D-SOR measurements show the highest reflectance (Fig. 3c). Above 0.5–0.6 V_{RHE}, the 2D-SOR intensity starts decreasing slowly with the increasing anodic polarization, and the onset of such decrease was previously shown to coincide with the removal of the herringbone reconstruction,[32] which occurs in conjunction with the adsorption of sulphate anions (SO_4^{2-} or HSO_4^-) (Figs. 4b, 4e) and potentially other oxygenated species, e.g. OH^-.[67,68,75] Furthermore, there can also be other simultaneous phenomena that might influence the 2D-SOR intensity in this potential region other than adsorption, e.g. the creation of Au nano-islands as a result of the herringbone lifting,[59,77] or changes in the optical reflectivity of a metallic surface due to the presence of an electric field.[78] Above 1.5 V_{RHE} the surface appears oxidized (Fig. 4c), as previously described, and it remains oxidized during the downward scan (Fig. 4d) until the reduction peak is approached.

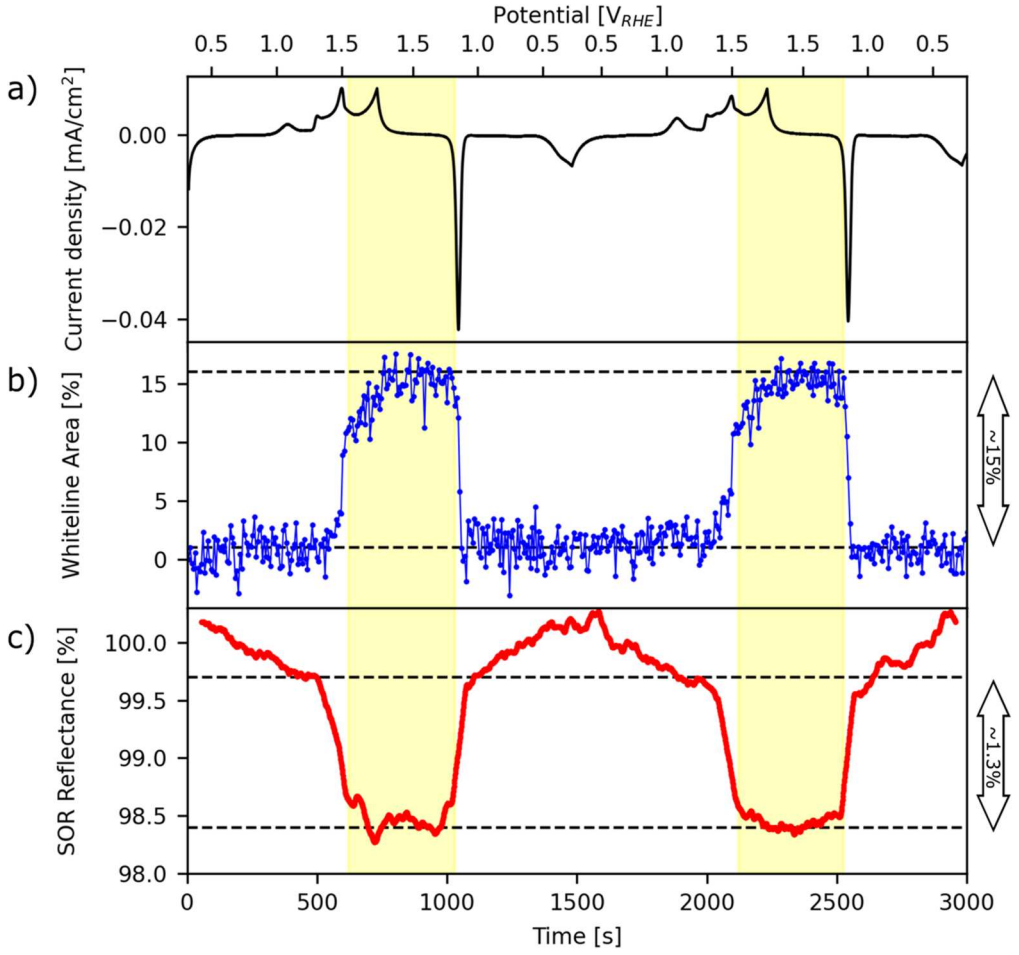

Figure 5. (a) Current density measured during two CV cycles on Au(111) in 0.05 M H_2SO_4 between 0.27 V_{RHE} and 1.77 V_{RHE} at 2 mV s^{-1}, plotted vs time. The first CV cycle corresponds to Fig. 3a. (b) RefleXAFS white line intensity, measured during the two CV cycles shown in panel a, plotted vs time. The white line intensity is normalized to the reference XANES intensity as in Fig. 3b. The yellow region indicates where the surface is clearly oxidized (above ~10% increase), according to the RefleXAFS signal. (c) 2D-SOR intensity measured during the two CV cycles, plotted vs time. The 2D-SOR intensity is normalized to the reflectance at OCP as in Fig. 3c.

Then, the (hydr-)oxide is reduced around 1.1 V_{RHE} and the 2D-SOR intensity in Fig. 3c steeply increases, but the surface is expected to be rougher and with smaller or no regions exhibiting the reconstructed surface[67,77,79] (Fig. 4f).

For a better comparison of the relative increase of the RefleXAFS white line intensity and the relative decrease of the 2D-SOR intensity over time, the results are summarised in Fig. 5 for both the CV cycles. The yellow region in Figs. 5a and 5b highlights where the surface is expected to be oxidized, while the dashed lines define the increase of the RefleXAFS white line intensity (∼15%) and the decrease of the 2D-SOR intensity (∼1.3%) due to surface oxidation. The dependence of the 2D-SOR intensity on the (hydr-)oxide thickness could be modelled with the Fresnel's equation [71,80,81] (Fig. S5). Using the refractive indexes of H_2O, bulk Au, and bulk Au_2O_3, we estimate a thickness of ∼5 Å, in good agreement with the previous XRR studies[75] and with the apparent thickness estimated from the reduction peak charge in Fig. S6 (∼6 Å). These values are also meaningful when compared to the intensity increase of the RefleXAFS white line intensity (∼15% increase): the X-rays penetration depth in the material in total reflection condition corresponds to 2–3 nm, suggesting that the (hydr-)oxide film formed below the onset of OER should correspond to only a few atomic layers.

Conclusions

We have followed the electro-oxidation and reduction of a Au(111) surface using RefleXAFS and 2D-SOR simultaneously during CV in 0.05 M H_2SO_4 at 2 mV s^{-1}, with a time resolution of one RefleXAFS spectrum measured every 5 s. Around 1.5 V_{RHE} during the anodic (upward) CV scan, a sudden increase of the Au L_3-edge white line intensity is observed in the RefleXAFS spectra which demostrate the formation of an ultra-thin Au^{3+} (hydr-)oxide film. The white line intensity does not further increase significantly, suggesting that the surface (hydr-)oxide shows a self-limiting thickness in this potential range. Similarly, the 2D-SOR intensity shows a significant decrease at the oxidation potential, that can be explained by a change of the surface refractive index during oxidation. The drop in the 2D-SOR signal can be used to estimate the ultra-thin surface (hydr-)oxide thickness: using the refractive index of a bulk Au_2O_3 oxide the self-limiting thickness of the film is ∼5 Å, in good agreement with previous XRR studies and with the presumed thickness obtained from the reduction peak charge. At low potentials, the RefleXAFS measurements do not show significant changes in the EDL region and during ORR. Instead, the 2D-SOR revealed a small, linear, intensity decrease with increasing polarization in this potential region which might be attributed to the adsorption/desorption of species and to the reconstruction of the surface, although the exact nature of these changes remains unknown. These results highlight the unique features of combined multimodal RefleXAFS and 2D-SOR, showing they can provide high surface sensitivity and reasonable time-resolution, in real *operando* conditions, independent of the sample thickness. Particularly, RefleXAFS measurements are not limited by the crystallinity of the sample and can outperform fluorescence-mode GI-XAFS measurements in terms of surface sensitivity. 2D-SOR has proven to be a powerful, relatively cheap and easy-to-use lab-scale tool giving complementary information to the RefleXAFS and CV experiments. Finally, we believe that these results can provide useful insights for electro-catalysts characterization and for fundamental studies on the behaviour of model electrodes in the field of electrocatalysis.

Acknowledgments

Financial support was acknowledged from the Swedish Research Council (2018-05374, 2022-04828, 2018–03434, 2020–06154 and 2022–03041) and the Swedish Foundation for Strategic Research under contract ID19–0032. The authors acknowledge MAX IV Laboratory for time at the Balder Beamline under Proposals 20221131 and 20220993. Research conducted at MAX IV, a Swedish national user facility, is supported by the Swedish Research council under contract 2018–07152, the Swedish Governmental Agency for Innovation Systems under contract 2018–04969, and Formas under contract 2019–02496.

ORCID

A. Grespi https://orcid.org/0000-0003-3132-4318
A. Larsson https://orcid.org/0000-0002-8932-8381
G. Abbondanza https://orcid.org/0000-0002-0680-5454
J. Manidi https://orcid.org/0000-0001-7171-1385
J. Eidhagen https://orcid.org/0000-0001-6830-5474
E. Lira https://orcid.org/0009-0008-7001-8480
A. Ti https://orcid.org/0009-0002-6601-116X
M. Ramakrishnan https://orcid.org/0000-0001-5384-9786
J. Just https://orcid.org/0000-0003-1725-1677
J. Pan https://orcid.org/0000-0002-4431-0671
L. R. Merte https://orcid.org/0000-0002-3213-4199
E. Lundgren https://orcid.org/0000-0002-3692-6142

References

1. O. Diaz-Morales, F. Calle-Vallejo, C. De Munck, and M. T. M. Koper, "Electrochemical water splitting by gold: Evidence for an oxide decomposition mechanism." *Chem. Sci.*, **4**, 2334 (2013).
2. N. T. T. Thao, J. U. Jang, A. K. Nayak, and H. Han, "Current trends of iridium-based catalysts for oxygen evolution reaction in acidic water electrolysis." *Small Sci.*, **4**, 2300109 (2024).
3. A. M. Gómez-Marín, R. Rizo, and J. M. Feliu, "Oxygen reduction reaction at Pt single crystals: A critical overview." *Catal. Sci. Technol.*, **4**, 1685 (2014).
4. M. Graf, M. Haensch, J. Carstens, G. Wittstock, and J. Weissmüller, "Electrocatalytic methanol oxidation with nanoporous gold: microstructure and selectivity." *Nanoscale*, **9**, 17839 (2017).
5. P. Rodriguez, D. Plana, D. J. Fermin, and M. T. M. Koper, "New insights into the catalytic activity of gold nanoparticles for CO oxidation in electrochemical media." *J. Catal.*, **311**, 182 (2014).
6. M. Pasta, F. La Mantia, and Y. Cui, "Mechanism of glucose electrochemical oxidation on gold surface." *Electrochim. Acta*, **55**, 5561 (2010).
7. N. P. Subramanian, T. A. Greszler, J. Zhang, W. Gu, and R. Makharia, "Pt-oxide coverage-dependent oxygen reduction reaction (ORR) kinetics." *J. Electrochem. Soc.*, **159**, B531 (2012).
8. M. P. J. M. Van Der Ham, E. Van Keulen, M. T. M. Koper, A. A. Tashvigh, and J. H. Bitter, "Steering the selectivity of electrocatalytic glucose oxidation by the Pt oxidation state." *Angew. Chem. Int. Ed.*, **62**, e202306701 (2023).
9. S. Cherevko, A. A. Topalov, A. R. Zeradjanin, I. Katsounaros, and K. J. J. Mayrhofer, "Gold dissolution: towards understanding of noble metal corrosion." *RSC Adv.*, **3**, 16516 (2013).
10. K. Stojanovski, V. Briega-Martos, M. Zlatar, C. Göllner, and S. Cherevko, "pH dependence of noble metals dissolution: Gold." *Chem. Electro. Chem.*, e202400373 (2024).
11. Y. Luo, Z. Zhang, M. Chhowalla, and B. Liu, "Recent advances in design of electrocatalysts for high-current-density water splitting." *Adv. Mater.*, **34**, 2108133 (2022).
12. J. Li, W. Tian, Q. Li, and S. Zhao, "Acidic oxygen evolution reaction: Fundamental understanding and electrocatalysts design." *Chem. Sus. Chem.*, **17**, e202400239 (2024).
13. W. Zhang, A. D. Bas, E. Ghali, and Y. Choi, "Passive behavior of gold in sulfuric acid medium." *Trans. Nonferrous Met. Soc. China*, **25**, 2037 (2015).
14. S. Anantharaj, S. Noda, M. Driess, and P. W. Menezes, "The pitfalls of using potentiodynamic polarization curves for tafel analysis in electrocatalytic water splitting." *ACS Energy Lett.*, 1607 (2021).
15. M. Zlatar et al., "Standardizing OER Electrocatalyst benchmarking in aqueous electrolytes: Comprehensive guidelines for accelerated stress tests and backing electrodes." *ACS Catal.*, **13**, 15375 (2023).
16. L. D'Amario, M. B. Stella, T. Edvinsson, M. Persico, J. Messinger, and H. Dau, "Towards time resolved characterization of electrochemical reactions: Electrochemically-induced raman spectroscopy." *Chem. Sci.*, **13**, 10734 (2022).
17. T. Fuchs, V. Briega-Martos, J. O. Fehrs, C. Qiu, M. Mirolo, C. Yuan, S. Cherevko, J. Drnec, O. M. Magnussen, and D. A. Harrington, "Driving force of the initial step in electrochemical Pt(111) oxidation." *J. Phys. Chem. Lett.*, **14**, 3589 (2023).
18. A. Larsson et al., "The oxygen evolution reaction drives passivity breakdown for Ni–Cr–Mo alloys." *Adv. Mater.*, 2304621 (2023).
19. O. M. Magnussen, J. Drnec, C. Qiu, I. Martens, J. J. Huang, R. Chattot, and A. Singer, "In situ and *operando* X-ray scattering methods in electrochemistry and electrocatalysis." *Chem. Rev.*, **124**, 629 (2024).
20. Y. Yang et al., "Operando methods: a new era of electrochemistry." *Curr. Opin. Electrochem.*, **42**, 101403 (2023).
21. E. Lundgren, C. Zhang, L. R. Merte, M. Shipilin, S. Blomberg, U. Hejral, J. Zhou, J. Zetterberg, and J. Gustafson, "Novel in situ techniques for studies of model catalysts." *Acc. Chem. Res.*, **50**, 2326 (2017).

22. O. M. Magnussen, "The rise of electrochemical surface science: From in situ interface structure to operando dynamics." *Surf. Sci.*, **749**, 122574 (2024).
23. J. Zetterberg, A. Larsson, A. Grespi, S. Pfaff, L. Rämisch, L. Merte, and E. Lundgren, "2D surface optical reflectance for use in harsh reactive environments." *J. Phys. Condens. Matter.*, **37**, 133003 (2025).
24. W. G. Onderwaater, A. Taranovskyy, G. C. Van Baarle, J. W. M. Frenken, and I. M. N. Groot, "In situ optical reflectance difference observations of CO oxidation over Pd(100)." *J. Phys. Chem. C*, **121**, 11407 (2017).
25. W. G. Onderwaater, A. Taranovskyy, G. M. Bremmer, G. C. Van Baarle, J. W. M. Frenken, and I. M. N. Groot, "From dull to shiny: a novel setup for reflectance difference analysis under catalytic conditions." *Rev. Sci. Instrum.*, **88**, 023704 (2017).
26. J. Gustafson, M. Shipilin, C. Zhang, A. Stierle, U. Hejral, U. Ruett, O. Gutowski, P.-A. Carlsson, M. Skoglundh, and E. Lundgren, "High-energy surface X-ray diffraction for fast surface structure determination." *Science*, **343**, 758 (2014).
27. S. Blomberg et al., "In situ X-ray photoelectron spectroscopy of model catalysts: at the edge of the gap." *Phys. Rev. Lett.*, **110**, 117601 (2013).
28. J. Knudsen et al., "Stroboscopic operando spectroscopy of the dynamics in heterogeneous catalysis by event-averaging." *Nat. Commun.*, **12**, 6117 (2021).
29. P. Li, M. Allain, T. A. Grünewald, M. Rommel, A. Campos, D. Carbone, and V. Chamard, "4th generation synchrotron source boosts crystalline imaging at the nanoscale." *Light: Sci. Appl.*, **11**, 73 (2022).
30. A. Larsson et al., "In situ quantitative analysis of electrochemical oxide film development on metal surfaces using ambient pressure X-ray photoelectron spectroscopy: industrial alloys." *Appl. Surf. Sci.*, **611**, 155714 (2023).
31. S. Kumar, J. J. C. Counter, D. C. Grinter, M. A. V. Spronsen, P. Ferrer, A. Large, M. W. Orzech, P. Jerzy Wojcik, and G. Held, "An electrochemical flow cell for operando XPS and NEXAFS Investigation of solid–liquid interfaces." *J. Phys.: Energy*, **6**, 036001 (2024).
32. W. Linpé et al., "Revisiting optical reflectance from Au(111) electrode surfaces with combined high-energy surface X-ray diffraction." *J. Electrochem. Soc.*, **168**, 096511 (2021).
33. A. Grespi, A. Larsson, G. Abbondanza, J. Eidhagen, D. Gajdek, J. Manidi, A. Tayal, J. Pan, L. R. Merte, and E. Lundgren, "Probing the electrode-liquid interface using operando total-reflection X-ray absorption spectroscopy." *Surf. Sci.*, **748**, 122538 (2024).
34. D. Hecht, P. Borthen, and H.-H. Strehblow, "An X-ray absorption fine structure study of the initial stages of the anodic oxidation of silver." *Surf. Sci.*, **365**, 263 (1996).
35. H. Abe, Y. Niwa, Y. Takeichi, and M. Kimura, "In situ TREXS observation of surface reduction reaction of NiO Film with ∼2 Nm surface sensitivity." *Chem. Rec.*, **19**, 1457 (2019).
36. A. Grespi et al., "An ultrathin hydroxide film governs the stability and reactivity of gold for the oxygen evolution reaction." *Chemistry* (2025), 10.26434/chemrxiv-2025-149tj.
37. D. Gajdek, P. A. T. Olsson, S. Blomberg, J. Gustafson, P.-A. Carlsson, D. Haase, E. Lundgren, and L. R. Merte, "Structural changes in monolayer cobalt oxides under ambient pressure CO and O_2 studied by in situ grazing-incidence X-ray absorption fine structure spectroscopy." *J. Phys. Chem. C*, **126**, 3411 (2022).
38. S. M. Gericke et al., "In situ H2 reduction of Al2O3-supported Ni- and Mo-based catalysts." *Catalysts*, **12**, 755 (2022).
39. L. G. Parratt, "Surface studies of solids by total reflection of X-rays." *Phys. Rev.*, **95**, 359 (1954).
40. G. Falkenberg, G. Pepponi, C. Streli, and P. Wobrauschek, "Comparison of conventional and total reflection excitation geometry for fluorescence X-ray absorption spectroscopy on droplet samples." *Spectrochim. Acta Part B At. Spectrosc.*, **58**, 2239 (2003).
41. D. K. G. De Boer, "Glancing-incidence X-ray fluorescence of layered materials." *Phys. Rev. B*, **44**, 498 (1991).
42. F. Meirer, A. Singh, P. Pianetta, G. Pepponi, F. Meirer, C. Streli, and T. Homma, "Synchrotron radiation-induced total reflection X-ray fluorescence analysis." *TrAC, Trends Anal. Chem.*, **29**, 479 (2010).
43. D. Friebel, D. J. Miller, D. Nordlund, H. Ogasawara, and A. Nilsson, "Degradation of bimetallic model electrocatalysts: An in situ X-Ray absorption spectroscopy study." *Angew. Chem. Int. Ed.*, **50**, 10190 (2011).
44. C. Maurizio, M. Rovezzi, F. Bardelli, H. G. Pais, and F. D'Acapito, "Setup for optimized grazing incidence X-ray absorption experiments on thin films on substrates." *Rev. Sci. Instrum.*, **80**, 063904 (2009).
45. W.-J. Chun, K. Asakura, and Y. Iwasawa, "Polarization-dependent total-reflection fluorescence XAFS study of Mo oxides on a rutile TiO_2 (110) single crystal surface." *J. Phys. Chem. B*, **102**, 9006 (1998).
46. D. Lützenkirchen-Hecht, J. Stötzel, J. Just, O. Müller, B. Bornmann, and R. Frahm, "Time-resolved grazing incidence X-Ray absorption spectroscopy for the in situ investigation of the initial stages of sputter-deposited copper thin films." *Phys. Status Solidi A*, **219**, 2100514 (2022).
47. H. Abe, T. Nakayama, Y. Niwa, H. Nitani, H. Kondoh, and M. Nomura, "Observation of surface reduction of NiO to Ni by surface-sensitive total reflection X-ray spectroscopy using kramers–kronig relations." *Jpn. J. Appl. Phys.*, **55**, 062401 (2016).
48. S. Pizzini, K. J. Roberts, G. N. Greaves, N. T. Barrett, I. Dring, and R. J. Oldman, "X-Ray absorption spectroscopy under conditions of total external reflection: Application to the structural characterisation of the Cu/GaAs(100) interface." *Faraday Discuss. Chem. Soc.*, **89**, 51 (1990).
49. G. Martens and P. Rabe, "EXAFS Studies on superficial regions by means of total reflection." *Phys. Status Solidi A*, **58**, 415 (1980).
50. D. Hecht, R. Frahm, and H.-H. Strehblow, "Quick-scanning EXAFS in the reflection mode as a probe for structural information of electrode surfaces with time resolution: an in situ study of anodic silver oxide formation." *J. Phys. Chem.*, **100**, 10831 (1996).
51. P. Rodriguez and M. T. M. Koper, "Electrocatalysis on gold." *Phys. Chem. Chem. Phys.*, **16**, 13583 (2014).
52. Z. Borkowska, A. Tymosiak-Zielinska, and G. Shul, "Electrooxidation of methanol on polycrystalline and single crystal gold electrodes." *Electrochim. Acta*, **49**, 1209 (2004).
53. B. B. Blizanac, M. Arenz, P. N. Ross, and N. M. Marković, "Surface electrochemistry of CO on reconstructed gold single crystal surfaces studied by infrared reflection absorption spectroscopy and rotating disk electrode." *J. Am. Chem. Soc.*, **126**, 10130 (2004).
54. R. R. Adzic, M. W. Hsiao, and E. B. Yeager, "Electrochemical oxidation of glucose on single crystal gold surfaces." *Journal of Electroanalytical Chemistry and Interfacial Electrochemistry*, **260**, 475 (1989).
55. A. Hamelin, "Cyclic voltammetry at gold single-crystal surfaces: Part 1. Behaviour at low-index faces." *J. Electroanal. Chem.*, **407**, 1 (1996).
56. C. Griesser, D. Winkler, T. Moser, L. Haug, M. Thaler, E. Portenkirchner, B. Klötzer, S. Diaz-Coello, E. Pastor, and J. KunzeLiebhäuser, "Lab-based electrochemical X-ray photoelectron spectroscopy for in-situ probing of redox processes at the electrified solid/liquid interface." *Electrochem. Sci. Adv.*, e2300007 (2023).
57. U. Zhumaev, A. V. Rudnev, J.-F. Li, A. Kuzume, T.-H. Vu, and T. Wandlowski, "Electro-oxidation of Au(111) in contact with aqueous electrolytes: New insight from in situ vibration spectroscopy." *Electrochim. Acta*, **112**, 853 (2013).
58. J. Drnec, D. A. Harrington, and O. M. Magnussen, "Electrooxidation of Pt(111) in acid solution." *Curr. Opin. Electrochem.*, **4**, 69 (2017).
59. M. Ruge, J. Drnec, B. Rahn, F. Reikowski, D. A. Harrington, F. Carlà, R. Felici, J. Stettner, and O. M. Magnussen, "Electrochemical oxidation of smooth and nanoscale rough Pt(111): an in situ surface X-ray scattering study." *J. Electrochem. Soc.*, **164**, H608 (2017).
60. S.-Y. Chang, A. Uehara, S. G. Booth, K. Ignatyev, J. F. W. Mosselmans, R. A. W. Dryfe, and S. L. M. Schroeder, "Structure and bonding in Au(I) chloride species: A critical examination of X-ray absorption spectroscopy (XAS) Data." *RSC Adv.*, **5**, 6912 (2015).
61. A. Pantelouris, G. Kueper, J. Hormes, C. Feldmann, and M. Jansen, "Anionic gold in Cs3AuO and Rb3AuO established by X-ray absorption spectroscopy." *J. Am. Chem. Soc.*, **117**, 11749 (1995).
62. J. Bansmann, G. Kučerová, A. M. Abdel-Mageed, A. Abd El-Moemen, and R. J. Behm, "Influence of re-activation and ongoing CO oxidation reaction on the chemical and electronic properties of Au on a Au/CeO 2 catalyst: A XANES study at the Au L III Edge." *J. Electron. Spectrosc. Relat. Phenom.*, **220**, 86 (2017).
63. M. L. Foresti, A. Pozzi, M. Innocenti, G. Pezzatini, F. Loglio, E. Salvietti, A. Giusti, F. D'Anca, R. Felici, and F. Borgatti, "In situ X-ray analysis under controlled potential conditions: An innovative setup and its application to the investigation of ultrathin films electrodeposited on Ag(111)." *Electrochim. Acta*, **51**, 5532 (2006).
64. W. Linpé, G. S. Harlow, A. Larsson, G. Abbondanza, L. Rämisch, S. Pfaff, J. Zetterberg, J. Evertsson, and E. Lundgren, "An electrochemical cell for 2-dimensional surface optical reflectance during anodization and cyclic voltammetry." *Rev. Sci. Instrum.*, **91**, 044101 (2020).
65. J. Timoshenko and B. Roldan Cuenya, "In situ/*operando* electrocatalyst characterization by X-ray absorption spectroscopy." *Chem. Rev.*, **121**, 882 (2021).
66. B. Ravel and M. Newville, "Athena, artemis, hephaestus: Data analysis for X-ray absorption spectroscopy using IFEFFIT." *J. Synchrotron Radiat.*, **12**, 537 (2005).
67. A. Cuesta, M. Kleinert, and D. M. Kolb, "The adsorption of sulfate and phosphate on Au(111) and Au(100) electrodes: An in situ STM study." *Phys. Chem. Chem. Phys.*, **2**, 5684 (2000).
68. A. Adnan, S. Behjati, N. Félez-Guerrero, K. Ojha, and M. T. M. Koper, "Tracking the surface structure and the influence of cations and anions on the double-layer region of a Au(111) electrode." *Phys. Chem. Chem. Phys.*, **26**, 21419 (2024).
69. X. Zhao and Y. Liu, "Origin of selective production of hydrogen peroxide by electrochemical oxygen reduction." *J. Am. Chem. Soc.*, **143**, 9423 (2021).
70. A. M. Gómez-Marín, A. Boronat, and J. M. Feliu, "Electrocatalytic oxidation and reduction of H2O2 on Au single crystals." *Russ. J. Electrochem.*, **53**, 1029 (2017).
71. S. Pfaff, A. Larsson, D. Orlov, G. S. Harlow, G. Abbondanza, W. Linpé, L. Rämisch, S. M. Gericke, J. Zetterberg, and E. Lundgren, "*Operando* reflectance microscopy on polycrystalline surfaces in thermal catalysis, electrocatalysis, and corrosion." *ACS Appl. Mater. Interfaces*, **13**, 19530 (2021).
72. K. Juodkazis, J. Juodkazyt, B. Šebeka, and A. Lukinskas, "Cyclic voltammetric studies on the reduction of a gold oxide surface layer." *Electrochem. Commun.*, **1**, 315 (1999).
73. J. T. Calla and R. J. Davis, "X-ray absorption spectroscopy and CO oxidation activity of Au/Al2O3 treated with NaCN." *Catal. Lett.*, **99**, 21 (2005).
74. C. M. Vitus and A. J. Davenport, "In situ scanning tunneling microscopy studies of the formation and reduction of a gold oxide monolayer on Au(111)." *J. Electrochem. Soc.*, **141**, 1291 (1994).
75. T. Kondo, J. Morita, K. Hanaoka, S. Takakusagi, K. Tamura, M. Takahasi, J. Mizuki, and K. Uosaki, "Structure of Au(111) and Au(100) single-crystal electrode surfaces at various potentials in sulfuric acid solution determined by in situ surface X-ray scattering." *J. Phys. Chem. C*, **111**, 13197 (2007).

76. K. Namink, X. Meng, M. T. M. Koper, P. Kukura, and S. Faez, "Electric-double-layer-modulation microscopy." *Phys. Rev. Appl.*, **13**, 044065 (2020).
77. S. Behjati and M. T. M. Koper, "In situ STM study of roughening of Au(111) Single-crystal electrode in sulfuric acid solution during oxidation–reduction cycles." *J. Phys. Chem. C*, **128**, 19024 (2024).
78. M. Cardona, K. L. Shaklee, and F. H. Pollak, "Electroreflectance at a semiconductor-electrolyte interface." *Phys. Rev.*, **154**, 696 (1967).
79. C. Stumm, S. Grau, F. D. Speck, F. Hilpert, V. Briega-Martos, K. Mayrhofer, S. Cherevko, O. Brummel, and J. Libuda, "Reduction of oxide layers on Au(111): The interplay between reduction rate, dissolution, and restructuring." *J. Phys. Chem. C*, **125**, 22698 (2021).
80. A. Larsson, M. Vorobyova, S. Pfaff, G. Abbondanza, J. Pan, J. Zetterberg, and E. Lundgren, "Operando surface optical reflectance microscopy study of corrosion film growth on a Ni–Cr–Mo alloy during anodic polarization." *J. Phys. Chem. C*, **127**, 21871 (2023).
81. L. Rämisch, S. M. Gericke, S. Pfaff, E. Lundgren, and J. Zetterberg, "Infrared surface spectroscopy and surface optical reflectance for operando catalyst surface characterization." *Appl. Surf. Sci.*, **578**, 152048 (2022).